Applied Physics Letters

RESEARCH ARTICLE | DECEMBER 16 2025

Dirac edge states as signature of two-dimensional altermagnetic topological crystalline phase

Special Collection: Quantum Geometry in Condensed Matter: Fundamentals and Applications

Raghottam M. Sattigeri ; Xujia Gong; Amar Fakhredine ; Carmine Autieri ; Giuseppe Cuono

Check for updates

Appl. Phys. Lett. 127, 243103 (2025)
https://doi.org/10.1063/5.0285433

View Online
Export Citation

Articles You May Be Interested In

Spin-dependent transport in altermagnet CrSb-based magnetic tunnel junction

Appl. Phys. Lett. (November 2025)

Nonlinear field dependence of Hall effect and high-mobility multi-carrier transport in an altermagnet CrSb

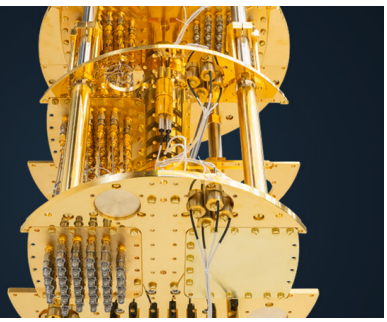
Appl. Phys. Lett. (January 2025)

Two-dimensional altermagnets from high throughput computational screening: Symmetry requirements, chiral magnons, and spin-orbit effects

Appl. Phys. Lett. (May 2024)

18 December 2025 09:06:25

BLUEFORS
More wiring. More qubits. More results.
The world's most popular fridge just got better.
Discover the new side-loading LD system



AIP Publishing

Applied Physics Letters ARTICLE pubs.aip.org/aip/apl

Dirac edge states as signature of two-dimensional altermagnetic topological crystalline phase

Cite as: Appl. Phys. Lett. **127**, 243103 (2025); doi: 10.1063/5.0285433
Submitted: 15 June 2025 · Accepted: 28 November 2025 ·
Published Online: 16 December 2025

View Online Export Citation CrossMark

Raghottam M. Sattigeri,[1,a)] Xujia Gong,[2] Amar Fakhredine,[2,3] Carmine Autieri,[2,4] and Giuseppe Cuono[5]

AFFILIATIONS

[1]Dipartimento di Fisica, Politecnico di Milano, Piazza Leonardo Da Vinci 32, Milano 20133, Italy
[2]International Research Centre Magtop, Institute of Physics, Polish Academy of Sciences, Aleja Lotników 32/46, 02668 Warsaw, Poland
[3]Institute of Physics, Polish Academy of Sciences, Aleja Lotników 32/46, 02668 Warsaw, Poland
[4]SPIN-CNR, UOS Salerno, IT-84084 Fisciano (SA), Italy
[5]Consiglio Nazionale delle Ricerche (CNR-SPIN), Unità di Ricerca presso Terzi c/o Università "G. D'Annunzio", 66100 Chieti, Italy

Note: This paper is part of the Special Topic, Quantum Geometry in Condensed Matter: Fundamentals and Applications.
[a)]**Author to whom correspondence should be addressed:** raghottam.sattigeri@polimi.it

ABSTRACT

Two-dimensional (2D) metallic altermagnets present exciting opportunities for both fundamental research and practical innovations. Their ability to enhance tunneling magnetoresistance in magnetic tunnel junctions, combined with the direct control of spin currents via electric fields, makes them highly promising for spintronic devices. Moreover, the rich electronic structure of altermagnets can host nontrivial topological phases. In particular, topological crystalline insulators are compounds where the topological states are protected by both crystalline and time-reversal symmetries. Furthermore, manipulating the state of a system between topological and trivial phases through external parameters unlocks new possibilities for quantum materials and advanced electronics. We show the edge states of a 2D metallic compound that displays signatures of an underlying altermagnetic topological crystalline phase, using as a representative example Cr_2BAl, a 2D MBene metallic altermagnet with a $d_{x^2-y^2}$ altermagnetic ordering. We find that the system can host an altermagnetic phase with extremely large "weak ferrimagnetism" which is sizeable also with light atoms, only with an in-plane component of the Néel vector. The electronic structure of Cr_2BAl presents multiple crossings in the vicinity of the Fermi level along [100]- and [010]-directions. When the spin–orbit coupling interaction is included, with the Néel vector along [001]-direction, this results in a pronounced peak in the spin Hall conductivity. The simulated Cr–B terminated [100] edge-projected band structure reveals Dirac dispersions at the bulk crossings, which are absent in Cr–Al terminations.

© 2025 Author(s). All article content, except where otherwise noted, is licensed under a Creative Commons Attribution (CC BY) license (https://creativecommons.org/licenses/by/4.0/). https://doi.org/10.1063/5.0285433

18 December 2025 09:06:25

Magnetic materials are widely studied for their applications. Ferromagnets exhibit net magnetization and spin-split bands, while antiferromagnets show zero net magnetization and spin-degenerate bands. Recently discovered altermagnets combine these properties, featuring spin-split bands in momentum space and zero net magnetization in real space.[1–3] This spin-splitting arises without spin–orbit coupling (SOC), making it non-relativistic. Symmetry-wise, antiferromagnets rely on inversion or translation symmetry, whereas altermagnets rely on rotational or mirror symmetries. Including SOC, altermagnets exhibit an anomalous Hall effect (AHE) even without ferromagnetic order,[4,5] with weak ferromagnetism dependent on the magnetic moment direction.[5,6] In systems with staggered Dzyaloshinskii–Moriya interaction, spin components orthogonal to the Néel vector can induce weak ferromagnetism or weak ferrimagnetism.[6] Thanks to these properties, altermagnets hold promise for spintronics and quantum information technologies.[7–11]

Altermagnetism has been experimentally observed in bulk materials[12,13] and it has been predicted in many three-dimensional (3D) compounds.[1,2,14–19] Achieving altermagnetism in two-dimensional (2D) materials is more challenging compared to 3D compounds. This is primarily because 2D systems are confined to a plane, allowing only in-plane (planar) spin–momentum locking. In contrast, 3D materials offer additional momentum components and allow for bulk spin–momentum locking. Furthermore, when we project the 3D Brillouin

zone (BZ) in a 2D one, the *k*-points with opposite spin-splitting can merge and cancel the altermagnetism.[20] Research is ongoing on 2D altermagnets, which can be very useful for many applications. Altermagnetism was predicted in RuF_4,[21] FeS[110],[22] and in ultrathin films of GdAlSi,[23] it was shown that Fe_2Se_2O and V_2SeTeO can present piezo-altermagnetism,[24,25] while it was experimentally realized in V_2Se_2O[26] and KV_2Se_2O.[27] 2D altermagnets can be used as electrodes in magnetic tunnel junctions (MTJs) to increase the tunneling magnetoresistance (TMR) effect.[7] Furthermore, it was demonstrated that some 2D antiferromagnets can be functionalized into altermagnets by using an external electric field[28,29] and it was shown that the breaking of time-reversal symmetry in the Fe-based superconducting chalchogenides can be due to altermagnetism,[29] highlighting the potential to explore the interplay between 2D altermagnetism, superconductivity, and topology. This scenario aligns with broader studies of superconducting phenomena in systems with unconventional magnetic orders.[30] It was shown that Cr-based 2D metal borides, namely MBenes layers, can be used in the design of 2D altermagnets promoting intriguing phenomena.[31,32]

Topological insulators are a distinct phase of matter with an insulating bulk and conductive surface or edge states protected by time-reversal symmetry.[33] These states feature a Dirac cone, mimicking the energy–momentum relation of relativistic particles. Topological crystalline insulators (TCIs) exhibit surface states that are protected by both time-reversal symmetry and crystalline symmetries.[34,35] Unlike topological insulators, which host a Dirac point at $\bar{\Gamma}$, TCIs exhibit it at other high-symmetry points of the surface BZ, depending on the crystal symmetry. The discovery of the TCI phase in SnTe and its alloys has fueled extensive research into their properties.[36] The mirror Chern number is a topological invariant that characterizes systems with mirror symmetry, ensuring the presence of protected edge states in topological crystalline insulators.[35]

Microscopic models for 2D d_{xy} or $d_{x^2-y^2}$ altermagnets have demonstrated the appearance of previously unobserved Dirac crossings protected by mirror symmetries between bands with the same spin orientation but located on opposite sub-lattices.[37,38] When the Néel vector is oriented perpendicular to the plane, the spin–orbit coupling induces a gap at these Dirac points, giving rise to mirror Chern bands, which enable the quantum spin Hall effect.[37] The symmetry conditions enabling topologically protected Dirac points in 2D altermagnets were studied.[39] Other topological properties were discussed in 3D altermagnets,[40] including topological features in the antiferromagnetic metallic ground state of the $FeSb_3$ skutterudite,[41] Dirac fermions in the altermagnet Ce_4Sb_3,[42] and the discovery of Weyl altermagnetism[43–46] in CrSb and GdAlSi using experimental methods like spin angle-resolved photoemission spectroscopy or *ab initio* simulations and models.

In this work, we aim to predict the properties of a 2D material, Cr_2BAl, which belongs to the altermagnetic family. Some members of this family were recently synthesized.[47] We employ Density Functional Theory (DFT) calculations to determine the electronic structure and magnetic properties of the 2D monolayer Cr_2BAl. The system belongs to the altermagnetic phase characterized by planar spin–momentum locking and a spin-group integer of 2 (P-2),[2] and exhibits a *d*-wave altermagnetic order, with Dirac edge states away from the $\bar{\Gamma}$ point; therefore, it displays the signatures of an underlying altermagnetic topological crystalline phase. While other works use microscopic models to analyze theoretically the topological properties, we investigate, by means of computational techniques, a material that can be experimentally realized. In the following, we present the computational details and the structural, electronic, and topological properties, concluding with the final remarks.

DFT was employed to compute the electronic structure, edge states, and spin Hall conductivity as implemented in Quantum ESPRESSO with post-processing using Wannier90 and WannierTools.[48–52] We used the scalar-relativistic norm-conserving Martins–Troullier pseudopotentials with generalized-gradient approximations and Perdew–Burke–Ernzerhof exchange–correlation functional with optimized kinetic energy cutoff of 80 Ry.[53,54] Full relativistic nonlinear core corrections were included in the pseudopotential to address spin–orbit coupling effects. A uniform Monkhorst–Pack grid of $10 \times 10 \times 1$ was used to represent *k*-points in the irreducible two-dimensional Brillouin zone (BZ) in all the calculations.[55] Moreover, van der Waals Grimme corrections were included in all the calculations to ensure an accurate energetic description of the system.[56] To accurately describe the *d*-orbital electrons of transition metals, the DFT+U Dudarev formalism has been employed, with the Hubbard U term to simulate the electron correlation effects by using $U = 4$ eV and ortho-atomic projections. We chose a reasonable value of the Coulomb repulsion U based on previous literature on strongly correlated Cr *d*-orbitals. The Coulomb repulsion on the Cr atoms is around 6 eV in the insulating systems.[57] However, in the metallic phase, Fermi screening reduces the electrostatic repulsion and the value of $U = 4$ eV (which we have used) is more commonly used in the literature.[58] Due to the metallicity, variations of the Coulomb repulsion do not significantly alter the band structure as shown in the supplementary material, Fig. S4. The density functional theory calculations were followed by Wannierization and disentanglement procedure, which involved the *d*-orbitals localized on Cr sites and the *p*-orbitals localized on B and Al sites using Wannier90. For the *d*-orbitals, we have considered only the majority electrons for each atom. The edge states and spin Hall conductivity were computed using the iterative Green's function method implemented in WannierTools.

The side and top views of the 2D Cr_2BAl monolayer are shown in Figs. 1(a) and 1(b). The Cr_2BAl unit cell comprises two chromium atoms, one boron atom, and one aluminum atom, forming a tetragonal magnetic space group (MSG) P4′m′m (BNS # 99.165, OG # 99.3.825). This structure consists of two layers: one composed of aluminum

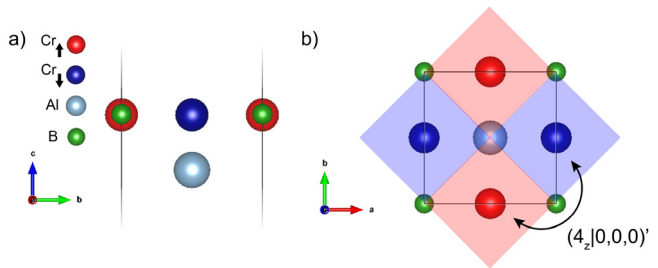


FIG. 1. Side view (a) and the top view (b) of the 2D Cr_2BAl unit cell. Chromium sub-lattices with opposite spin polarization are distinguished by blue and red spheres, boron atoms by green spheres, and aluminum by gray spheres. The rectangle and arrow in blue and purple highlight the generators of opposite-spin sub-lattice rotations. Here, the rotational operation was labeled using Litvin's notation $(4_z|\,0,0,0)'$.

18 December 2025 09:06:25

© Author(s) 2025

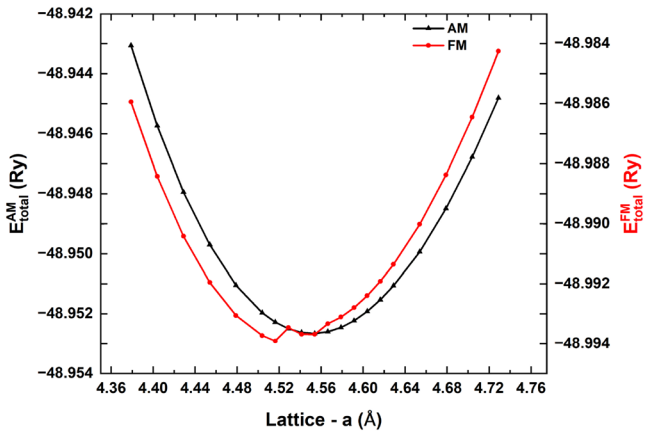


FIG. 2. The total energy for both the AM and FM configurations as a function of the lattice parameter *a*. The AM configuration exhibits a lower energy at around 4.54 Å, indicating a more stable magnetic ground state. A biaxial strain in the a–b plane can induce an altermagnet–ferromagnet transition.

atoms and the other composed of chromium and boron atoms, which have minimal difference in their *z*-coordinates. The two chromium atoms within the unit cell belong to different sub-lattices, denoted as $Cr_{\uparrow}$ (red) and $Cr_{\downarrow}$ (blue) as shown in Fig. 1(b). Each chromium atom exhibits a magnetic moment of 4.095 μ_B along the easy axis in the [001]-direction (out-of-plane), with a magnetic anisotropy energy (MAE) of 81 μ eV per f.u. This is relatively high due to the anisotropy of the 2D system, indeed, the MAE is an order of magnitude higher than that of some conventional bulk magnetic materials like Fe (1.4 μ eV per atom) and Ni (2.7 μ eV per atom), indicating the magnetic moment is stably maintained along the easy axis and allowing the long-range magnetic order to persist at finite temperature.[59,60] We performed a scan of the energies of the altermagnetic (AM) and ferromagnetic (FM) configurations as a function of the lattice constant *a*, as reported in Fig. 2. There is a broad range of values of *a* where the AM configuration is the ground state, with some local minima observed in the FM configurations.

Unlike conventional antiferromagnets, where sub-lattices with opposite spin polarization are coupled by translation and/or inversion symmetries, the sub-lattices in this system are coupled by mirror and rotational symmetries. This results in an electronic structure that breaks time-reversal ($\mathcal{T}$) symmetry, leading to alternating spin polarization in both coordinate and momentum spaces.[61,62] The electronic band structure is shown in Fig. 3(a), exhibiting a typical altermagnetic pattern given that the $\mathcal{T}$ symmetry is broken. The electronic bands are highly spin-split along Γ-X and Γ-Y, which is expected to generate large TMR, while they are degenerate along Γ-M. The system is metallic and it presents a $d_{x^2-y^2}$-wave altermagnetism, with opposite spin-splitting along Γ-X and Γ-Y. We show in Figs. 3(b) and 3(c) the bands with SOC and Fermi surfaces, where it can be seen that they are linked by rotational symmetry.

Although the SOC strength of Cr is not as high as in conventional heavy elements, it is not negligible either. We find that, in the non-relativistic regime, the altermagnetic bands [see Fig. 3(a)] possess multiple crossings in the vicinity of the Fermi level along [100]- and [010]-directions. This mandates a follow-up investigation of the influence of spin–orbital interactions, leading to insights into spin transport

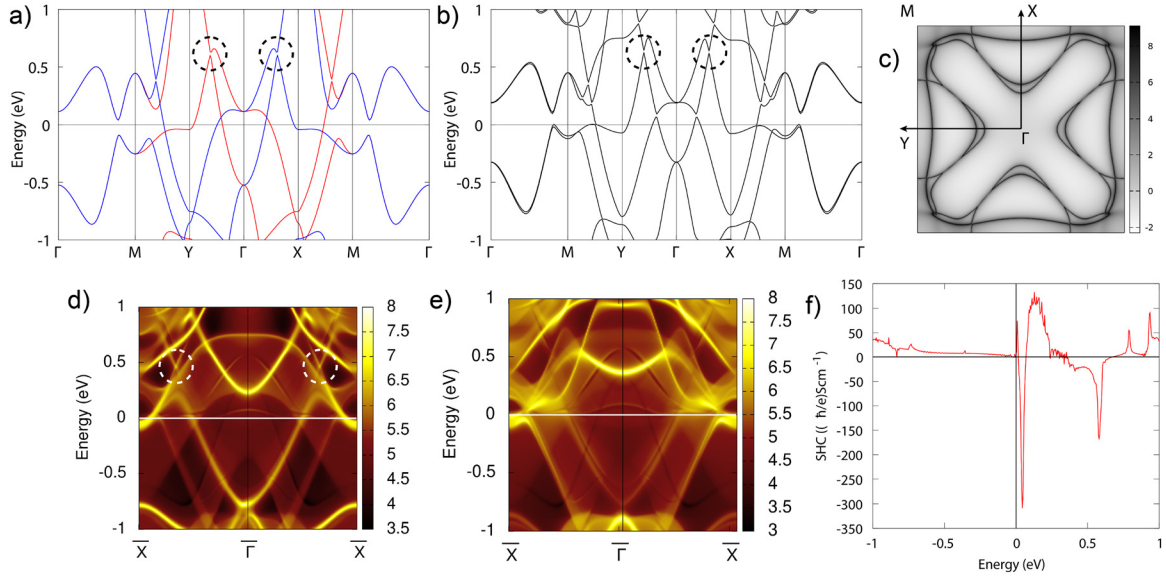


FIG. 3. (a) Non-relativistic spin-splitting (red: spin-up; blue: spin-down) in electronic band structure for the Cr_2BAl monolayer with band crossings (highlighted by dashed circles) along the BZ path X-Γ-Y, i.e., in [100]- and [010]-directions. (b) The electronic structure obtained with spin–orbit coupling (with the Néel vector in [001]-direction) with band crossings highlighted by dashed circles along the BZ path X-Γ-Y, i.e., in [100]- and [010]-directions. (c) Fermi surface slice in the 2D BZ, corresponding to the spin–orbit coupling bands presented in (b). Surface-projected band structure obtained using surface projections in [100]-direction: (d) The Cr–B surface termination indicates the presence of Dirac dispersions (highlighted by dashed circles) which coincide with the crossings observed in (b), leading to the peak in spin Hall conductivity at ∼525 meV observed in (f). (e) The Cr–Al surface termination, on the contrary, indicates the absence of Dirac dispersions. (f) The spin Hall conductivity indicating sharp peaks at ∼525 and ∼100 meV, corresponding to the multiple band crossings presented (a) and (b). The Fermi level is set to zero in all plots.

18 December 2025 09:06:25

© Author(s) 2025

phenomena such as spin Hall conductivity. With this objective in mind, we performed band structure calculations in the presence of SOC interactions. Since it was shown that the behavior of these crossings when SOC is introduced depends on the direction of the Néel vector, with topological bands with linear dispersions appearing for an out-of-plane Néel vector, we focus on the case when its direction is along [001].[37] The electronic band structure in the presence of SOC and with the Néel vector along [001]-direction is presented in Fig. 3(b). We observe a clear signature of Dirac dispersions from angle resolved photoemission spectroscopy (ARPES) like edge states projected onto the [100] surface, as shown in Fig. 3(d). However, it is important to note that surface terminations are vital in such cases. We can see that the Dirac dispersions persist only for Cr–B terminations, whereas they are absent for Cr–Al terminations [see Fig. 3(e)]. The system shows edge states as a signature of an altermagnetic topological crystalline phase,[35,36] and this manifests as peaks in the spin Hall conductivity plot, which is calculated as a function of the energy and presented in Fig. 3(f). It is worth mentioning that the calculation of a topological invariant, such as the Chern number, requires an energy gap separating valence and conduction bands. In our case, the system is metallic and therefore the topological invariant cannot be rigorously defined. This is the reason why we speak about the signature of a topological crystalline phase.

The non-relativistic spin-splitting phenomena observed in altermagnetic materials are governed by the direction of the Néel vector, especially in materials where SOC interactions are non-negligible. The spin canting effects originating from Dzyaloshinskii–Moriya interactions need to be addressed since they give rise to weak ferromagnetism or ferrimagnetism, depending on the presence or absence of centrosymmetry in the material, respectively.[6] Cr_2BAl is governed by tetragonal symmetry, which implies an absence of centrosymmetry. Using the same technique on the spin density of state developed by us to study the spin–orbital effect in altermagnets,[6] we demonstrate the presence of weak ferrimagnetism in this system only with the in-plane component of the Néel vector. First, we calculate the spin density for the spins along the [001]-direction represented in Fig. 4(a). The spin densities of S_z for $Cr_\uparrow$ and $Cr_\downarrow$ are equal and opposite, while there is no spin density along other directions (meaning that no spin cantings are allowed); therefore, we have an altermagnet with zero magnetization in the relativistic limit. We turn the Néel vector along the [100]-direction and we obtain the spin density reported in Fig. 4(b). The spins S_x of $Cr_\uparrow$ and $Cr_\downarrow$ are not equal and opposite; therefore, we have two different spins while the other spin components are zero (meaning that no spin cantings are allowed). We define E as the operator identity and M_y as the mirror operator for the y-axis. While the Néel vector along x preserves the combined antiunitary symmetry $[E||M_y]$, which includes the time-reversal symmetry, one of the Cr spins points toward the B atoms and one toward the Al atoms; these local environments are crystallographically inequivalent, which leads to observable differences in the spin-projected DOS when we add SOC. In Fig. 4(c), we plot the average and the difference of the spin densities of $Cr_\uparrow$ and $Cr_\downarrow$ such that the difference is the part related to the weak ferrimagnetism. While most of the altermagnets host only weak ferromagnetism, this altermagnet can host weak ferrimagnetism when the Néel vector is along the [100]-direction, while it exhibits weak ferromagnetism with the Néel vector along the [110]-direction.[37] The weak ferrimagnetism is around one order of magnitude smaller than the average spin density of states; therefore, this is larger than that observed in previously investigated weak ferromagnets like RuO_2, wurtzite MnSe,[6] and MnTe.[63] Despite the involvement of light element, this pronounced relativistic effect arises from the crystal symmetries.

In summary, we investigated the structural, electronic, magnetic, and topological properties of the MBene Cr_2BAl monolayer. We found that the Cr_2BAl monolayer exhibits an altermagnetic ground state over a wide range of lattice parameter values. Moreover, applying biaxial strain in the a–b plane can induce a transition from the altermagnetic to a ferromagnetic phase, highlighting the tunability of its magnetic order via lattice deformation. In this configuration, Cr_2BAl is a $d_{x^2-y^2}$ altermagnet, showing a non-relativistic spin-splitting in the band structure, with opposite splitting along Γ-X and Γ-Y and with degenerate bands along Γ-M. When the SOC interaction is included and when the Néel vector is along the [100]-direction, the system hosts a large weak ferrimagnetism compared to other investigated altermagnets due to crystal symmetries, despite the presence of light elements. Even if the system is metallic, it clearly shows the signatures of an underlying altermagnetic topological crystalline phase, with peaks in the spin Hall conductivity and Dirac dispersions visible along the [100] surface. Building on our findings, the Cr_2BAl monolayer emerges as a promising platform for next-generation spintronic and quantum devices, particularly due to its altermagnetic properties and topological features. Given its non-relativistic spin-splitting and zero net magnetization, it could be effectively utilized in MTJs to enhance the TMR effect, as it was already shown in other Cr-based MBenes.[32] Our investigations with SOC interactions further support the fact that Cr_2BAl can be explored experimentally for spintronic applications; however, the importance of surface terminations is essential to realize efficient performance in experimental scenarios.

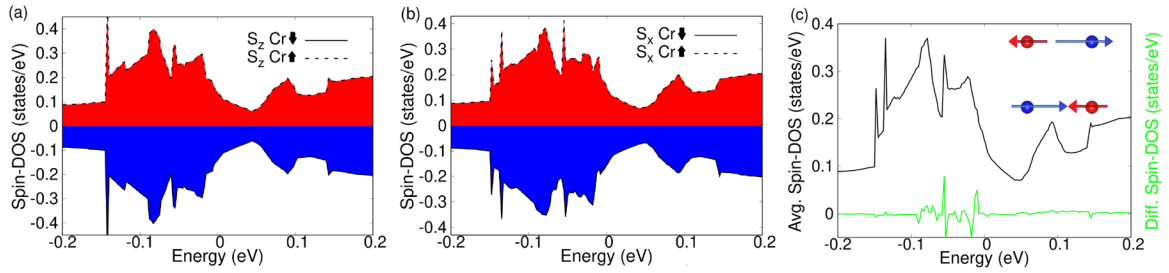


FIG. 4. Spin density of states of $Cr_\uparrow$ and $Cr_\downarrow$ at low energy for Cr_2BAl with Néel vector (a) along the [001]-direction and (b) along the [100]-direction. (c) Average spin density and difference in the spin density for the Néel vector along the [100]-direction. In the inset of panel (c), we present the magnetic spin configuration; the difference between the spins is exaggerated for graphical purposes. The difference between the spin densities of $Cr_\uparrow$ and $Cr_\downarrow$ represents the hallmark of weak ferrimagnetism.

18 December 2025 09:06:25

© Author(s) 2025

See the supplementary material for additional details, including phonon dispersion curves, comparisons of energetic stability with other antiferromagnetic configurations, and Wannierization data.

We thank W. Sun for valuable discussions. This research was supported by the "MagTop" project (FENG.02.01-IP.05-0028/23) carried out within the "International Research Agendas" program of the Foundation for Polish Science, co-financed by the European Union under the European Funds for Smart Economy 2021–2027 (FENG). C.A. and G.C. acknowledge receiving support from PNRR MUR project PE0000023-NQSTI. We further acknowledge access to the computing facilities of the Interdisciplinary Center of Modeling at the University of Warsaw, Grant g91-1418, g91-1419, g96-1808, and g96-1809 for the availability of high-performance computing resources and support. We acknowledge receiving access to the computing facilities of the Poznan Supercomputing and Networking Center, Grants No. pl0267-01, pl0365-01, and pl0471-01. R.M.S. acknowledges receiving the CINECA award under the ISCRA initiative IsCc4 "CHARPH2," IsCb7 "CHARPHEN," IsCc1 "DRIFT," and IsB29 "DASP" grants.

AUTHOR DECLARATIONS

Conflict of Interest

The authors have no conflicts to disclose.

Author Contributions

Raghottam M. Sattigeri: Conceptualization (equal); Formal analysis (equal); Investigation (lead); Methodology (lead); Visualization (equal); Writing – original draft (equal); Writing – review & editing (equal). **Xujia Gong:** Conceptualization (equal); Visualization (equal); Writing – review & editing (equal). **Amar Fakhredine:** Conceptualization (equal); Visualization (equal); Writing – review & editing (equal). **Carmine Autieri:** Conceptualization (equal); Formal analysis (equal); Writing – original draft (equal); Writing – review & editing (equal). **Giuseppe Cuono:** Conceptualization (equal); Formal analysis (equal); Writing – original draft (equal); Writing – review & editing (equal).

DATA AVAILABILITY

The data that support the findings of this study are available within the article and its supplementary material.

REFERENCES

[1]L. Šmejkal, J. Sinova, and T. Jungwirth, "Emerging research landscape of altermagnetism," Phys. Rev. X **12**, 040501 (2022).
[2]L. Šmejkal, J. Sinova, and T. Jungwirth, "Beyond conventional ferromagnetism and antiferromagnetism: A phase with nonrelativistic spin and crystal rotation symmetry," Phys. Rev. X **12**, 031042 (2022).
[3]I. Mazin and PRX editors, "Altermagnetism—A new punch line of fundamental magnetism," Phys. Rev. X **12**, 040002 (2022).
[4]L. Šmejkal, R. González-Hernández, T. Jungwirth, and J. Sinova, "Crystal time-reversal symmetry breaking and spontaneous Hall effect in collinear antiferromagnets," Sci. Adv. **6**, eaaz8809 (2020).
[5]D.-F. Shao, S.-H. Zhang, G. Gurung, W. Yang, and E. Y. Tsymbal, "Nonlinear anomalous Hall effect for Néel vector detection," Phys. Rev. Lett. **124**, 067203 (2020).
[6]C. Autieri, R. M. Sattigeri, G. Cuono, and A. Fakhredine, "Staggered Dzyaloshinskii-Moriya interaction inducing weak ferromagnetism in centrosymmetric altermagnets and weak ferrimagnetism in noncentrosymmetric altermagnets," Phys. Rev. B **111**, 054442 (2025).
[7]D.-F. Shao, S.-H. Zhang, M. Li, C.-B. Eom, and E. Y. Tsymbal, "Spin-neutral currents for spintronics," Nat. Commun. **12**, 7061 (2021).
[8]R. González-Hernández, L. Šmejkal, K. Výborný, Y. Yahagi, J. Sinova, T. Jungwirth, and J. Železný, "Efficient electrical spin splitter based on nonrelativistic collinear antiferromagnetism," Phys. Rev. Lett. **126**, 127701 (2021).
[9]L. Šmejkal, A. B. Hellenes, R. González-Hernández, J. Sinova, and T. Jungwirth, "Giant and tunneling magnetoresistance in unconventional collinear antiferromagnets with nonrelativistic spin-momentum coupling," Phys. Rev. X **12**, 011028 (2022).
[10]X. Zhou, W. Feng, R.-W. Zhang, L. Šmejkal, J. Sinova, Y. Mokrousov, and Y. Yao, "Crystal thermal transport in altermagnetic RuO_2," Phys. Rev. Lett. **132**, 056701 (2024).
[11]J. A. Ouassou, A. Brataas, and J. Linder, "DC Josephson effect in altermagnets," Phys. Rev. Lett. **131**(7), 076003 (2023).
[12]J. Krempaský, L. Šmejkal, S. D'Souza, M. Hajlaoui, G. Springholz, K. Uhlířová, F. Alarab, P. Constantinou, V. Strocov, D. Usanov *et al.*, "Altermagnetic lifting of Kramers spin degeneracy," Nature **626**, 517–522 (2024).
[13]Y.-P. Zhu, X. Chen, X.-R. Liu, Y. Liu, P. Liu, H. Zha, G. Qu, C. Hong, J. Li, Z. Jiang *et al.*, "Observation of plaid-like spin splitting in a noncoplanar antiferromagnet," Nature **626**, 523–528 (2024).
[14]L. Šmejkal, A. Marmodoro, K.-H. Ahn, R. González-Hernández, I. Turek, S. Mankovsky, H. Ebert, S. W. D'Souza, O. Šipr, J. Sinova, and T. Jungwirth, "Chiral magnons in altermagnetic RuO_2," Phys. Rev. Lett. **131**, 256703 (2023).
[15]I. I. Mazin, K. Koepernik, M. D. Johannes, R. González-Hernández, and L. Šmejkal, "Prediction of unconventional magnetism in doped $FeSb_2$," Proc. Natl. Acad. Sci. **118**, e2108924118 (2021).
[16]I. I. Mazin, "Altermagnetism in MnTe: Origin, predicted manifestations, and routes to detwinning," Phys. Rev. B **107**, L100418 (2023).
[17]G. Cuono, R. M. Sattigeri, J. Skolimowski, and C. Autieri, "Orbital-selective altermagnetism and correlation-enhanced spin-splitting in strongly-correlated transition metal oxides," J. Magn. Magn. Mater. **586**, 171163 (2023).
[18]A. Fakhredine, R. M. Sattigeri, G. Cuono, and C. Autieri, "Interplay between altermagnetism and nonsymmorphic symmetries generating large anomalous Hall conductivity by semi-Dirac points induced anticrossings," Phys. Rev. B **108**, 115138 (2023).
[19]M. J. Grzybowski, C. Autieri, J. Domagala, C. Krasucki, A. Kaleta, S. Kret, K. Gas, M. Sawicki, R. Bożek, J. Suffczyński, and W. Pacuski, "Wurtzite vs. rocksalt MnSe epitaxy: Electronic and altermagnetic properties," Nanoscale **16**, 6259–6267 (2024).
[20]R. M. Sattigeri, G. Cuono, and C. Autieri, "Altermagnetic surface states: Towards the observation and utilization of altermagnetism in thin films, interfaces and topological materials," Nanoscale **15**, 16998–17005 (2023).
[21]M. Milivojevic, M. Orozovic, S. Picozzi, M. Gmitra, and S. Stavric, "Interplay of altermagnetism and weak ferromagnetism in two-dimensional RuF_4," 2D Mater. **11**, 035025 (2024).
[22]Q. Liu, J. Kang, P. Wang, W. Gao, Y. Qi, J. Zhao, and X. Jiang, "Inverse magnetocaloric effect in altermagnetic 2D non-van der Waals FeX (X = S and Se) semiconductors," Adv. Funct. Mater. **34**, 2402080 (2024).
[23]O. E. Parfenov, D. V. Averyanov, I. S. Sokolov, A. N. Mihalyuk, O. A. Kondratev, A. N. Taldenkov, A. M. Tokmachev, and V. G. Storchak, "Pushing an altermagnet to the ultimate 2D limit: Symmetry breaking in monolayers of GdAlSi," J. Am. Chem. Soc. **147**, 5911–5920 (2025).
[24]Y. Zhu, T. Chen, Y. Li, L. Qiao, X. Ma, X. Ma, C. Liu, T. Hu, H. Gao, and W. Ren, "Multipiezo effect in altermagnetic V_2SeTeO monolayer," Nano Lett. **24**, 472–478 (2024).
[25]Y. Wu, L. Deng, X. Yin, J. Tong, F. Tian, and X. Zhang, "Valley-related multipiezo effect and noncollinear spin current in an altermagnet Fe_2Se_2O monolayer," Nano Lett. **24**, 10534–10539 (2024).
[26]H.-Y. Ma, M. Hu, N. Li, J. Liu, W. Yao, J.-F. Jia, and J. Liu, "Multifunctional antiferromagnetic materials with giant piezomagnetism and noncollinear spin current," Nat. Commun. **12**, 2846 (2021).
[27]B. Jiang, M. Hu, J. Bai, Z. Song, C. Mu, G. Qu, W. Li, W. Zhu, H. Pi, Z. Wei, Y. Sun, Y. Huang, X. Zheng, Y. Peng, L. He, S. Li, J. Luo, Z. Li, G. Chen, H. Li, H. Weng, and T. Qian, "A metallic room-temperature D-wave altermagnet," Nat. Phys. **21**, 754–759 (2025).

18 December 2025 09:06:25

© Author(s) 2025

[28]D. Wang, H. Wang, L. Liu, J. Zhang, and H. Zhang, "Electric-field-induced switchable two-dimensional altermagnets," Nano Lett. **25**, 498 (2025).
[29]I. Mazin, R. González-Hernández, and L. Šmejkal, "Induced monolayer altermagnetism in MnP(S,Se)$_3$ and FeSe," arXiv:2309.02355 (2023).
[30]Y. Fukaya, B. Lu, K. Yada, Y. Tanaka, and J. Cayao, "Superconducting phenomena in systems with unconventional magnets," J. Phys.: Condens. Matter **37**, 313003 (2025).
[31]J. Gu, Z. Zhao, J. Huang, B. G. Sumpter, and Z. Chen, "MX anti-MXenes from non-van der Waals bulks for electrochemical applications: The merit of metallicity and active basal plane," ACS Nano **15**, 6233–6242 (2021).
[32]W. Sun, M. Wang, B. Sa, S. Dong, and C. Autieri, "Altermagnetizing the FeSe-like two-dimensional materials and approaching to giant tunneling magnetoresistance with Janus Cr4BN(B2) MBene electrode," arXiv:2502.03165 (2025).
[33]M. Z. Hasan and C. L. Kane, "Colloquium: Topological insulators," Rev. Mod. Phys. **82**, 3045–3067 (2010).
[34]L. Fu, "Topological crystalline insulators," Phys. Rev. Lett. **106**, 106802 (2011).
[35]T. H. Hsieh, H. Lin, J. Liu, W. Duan, A. Bansil, and L. Fu, "Topological crystalline insulators in the SnTe material class," Nat. Commun. **3**, 1–7 (2012).
[36]P. Dziawa, B. Kowalski, K. Dybko, R. Buczko, A. Szczerbakow, M. Szot, E. Łusakowska, T. Balasubramanian, B. M. Wojek, M. Berntsen *et al.*, "Topological crystalline insulator states in $Pb_{1-x}Sn_xSe$," Nat. Mater. **11**, 1023–1027 (2012).
[37]D. S. Antonenko, R. M. Fernandes, and J. W. F. Venderbos, "Mirror Chern bands and Weyl nodal loops in altermagnets," Phys. Rev. Lett. **134**, 096703 (2025).
[38]L. Del Re, "Dirac points and topological phases in correlated altermagnets," Phys. Rev. Res. **7**, 033234 (2025).
[39]K. Parshukov, R. Wiedmann, and A. P. Schnyder, "Topological crossings in two-dimensional altermagnets: Symmetry classification and topological responses," Phys. Rev. B **111**, 224406 (2025).
[40]H.-Y. Ma and J.-F. Jia, "Altermagnetic topological insulator with C-paired spin-valley locking," Quantum Front. **3**, 22 (2024).
[41]E. D. Lucente, F. J. dos Santos, and N. Marzari, "Spin fluctuations steer electronic behavior and altermagnetism in the $FeSb_3$ skutterudite," arXiv:2501.15961 (2025).
[42]X. He and S. Zhang, "Dirac fermions in the altermagnet Ce_4Sb_3," Phys. Rev. B **112**, 075138 (2025).
[43]C. Li, M. Hu, Z. Li, Y. Wang, W. Chen, B. Thiagarajan, M. Leandersson, C. Polley, T. Kim, H. Liu, C. Fulga, M. G. Vergniory, O. Janson, O. Tjernberg, and J. van den Brink, "Topological Weyl altermagnetism in CrSb," Commun. Phys. **8**, 311 (2025).
[44]W. Lu, S. Feng, Y. Wang, D. Chen, Z. Lin, X. Liang, S. Liu, W. Feng, K. Yamagami, J. Liu, C. Felser, Q. Wu, and J. Ma, "Signature of topological surface bands in altermagnetic Weyl semimetal CrSb," Nano Lett. **25**, 7343 (2025).
[45]J. Nag, B. Das, S. Bhowal, Y. Nishioka, B. Bandyopadhyay, S. Sarker, S. Kumar, K. Kuroda, V. Gopalan, A. Kimura, K. G. Suresh, and A. Alam, "GdAlSi: An antiferromagnetic topological Weyl semimetal with nonrelativistic spin splitting," Phys. Rev. B **110**, 224436 (2024).
[46]S. Qu, X.-Y. Hou, Z.-X. Liu, P.-J. Guo, and Z.-Y. Lu, "Altermagnetic Weyl node-network metals protected by spin symmetry," Phys. Rev. B **111**, 195138 (2025).
[47]P. J. Pöllmann, S. Lellig, D. Bogdanovski, A. H. Navidi Kashani, D. M. Holzapfel, C. Azina, P. Schweizer, M. Hans, P. Zöll, D. Primetzhofer, S. Kolozsvári, P. Polcik, J. Michler, and J. M. Schneider, "Contactless tracking of decomposition in self-reporting ceramic Cr-Al-B coatings," Adv. Mater. Interfaces **12**, 2500092 (2025).
[48]P. Giannozzi, O. Andreussi, T. Brumme, O. Bunau, M. Buongiorno Nardelli, M. Calandra, R. Car, C. Cavazzoni, D. Ceresoli, M. Cococcioni, N. Colonna, I. Carnimeo, A. Dal Corso, S. de Gironcoli, P. Delugas, R. A. DiStasio, A. Ferretti, A. Floris, G. Fratesi, G. Fugallo, R. Gebauer, U. Gerstmann, F. Giustino, T. Gorni, J. Jia, M. Kawamura, H.-Y. Ko, A. Kokalj, E. Küçükbenli, M. Lazzeri, M. Marsili, N. Marzari, F. Mauri, N. L. Nguyen, H.-V. Nguyen, A. Otero-de-la Roza, L. Paulatto, S. Poncé, D. Rocca, R. Sabatini, B. Santra, M. Schlipf, A. P. Seitsonen, A. Smogunov, I. Timrov, T. Thonhauser, P. Umari, N. Vast, X. Wu, and S. Baroni, "Advanced capabilities for materials modelling with quantum espresso," J. Phys.: Condens. Matter **29**, 465901 (2017).
[49]N. Marzari, A. A. Mostofi, J. R. Yates, I. Souza, and D. Vanderbilt, "Maximally localized Wannier functions: Theory and applications," Rev. Mod. Phys. **84**, 1419–1475 (2012).
[50]A. A. Mostofi, J. R. Yates, G. Pizzi, Y.-S. Lee, I. Souza, D. Vanderbilt, and N. Marzari, "An updated version of wannier90: A tool for obtaining maximally-localised Wannier functions," Comput. Phys. Commun. **185**, 2309–2310 (2014).
[51]Q. Wu, S. Zhang, H.-F. Song, M. Troyer, and A. A. Soluyanov, "Wanniertools: An open-source software package for novel topological materials," Comput. Phys. Commun. **224**, 405–416 (2018).
[52]M. L. Sancho, J. L. Sancho, J. L. Sancho, and J. Rubio, "Highly convergent schemes for the calculation of bulk and surface green functions," J. Phys. F: Met. Phys. **15**, 851 (1985).
[53]P. E. Blöchl, "Projector augmented-wave method," Phys. Rev. B **50**, 17953–17979 (1994).
[54]J. P. Perdew, K. Burke, and M. Ernzerhof, "Generalized gradient approximation made simple," Phys. Rev. Lett. **77**, 3865–3868 (1996).
[55]H. J. Monkhorst and J. D. Pack, "Special points for Brillouin-zone integrations," Phys. Rev. B **13**, 5188–5192 (1976).
[56]S. Grimme, "Semiempirical GGA-type density functional constructed with a long-range dispersion correction," J. Comput. Chem. **27**, 1787–1799 (2006).
[57]C. Autieri, E. Koch, and E. Pavarini, "Mechanism of structural phase transitions in $KCrF_3$," Phys. Rev. B **89**, 155109 (2014).
[58]S. Pakdel, T. Olsen, and K. S. Thygesen, "Effect of Hubbard U-corrections on the electronic and magnetic properties of 2D materials: A high-throughput study," npj Comput. Mater. **11**, 18 (2025).
[59]G. H. O. Daalderop, P. J. Kelly, and M. F. H. Schuurmans, "First-principles calculation of the magnetocrystalline anisotropy energy of iron, cobalt, and nickel," Phys. Rev. B **41**, 11919–11937 (1990).
[60]Y. Fang, S. Wu, Z.-Z. Zhu, and G.-Y. Guo, "Large magneto-optical effects and magnetic anisotropy energy in two-dimensional $Cr_2Ge_2Te_6$," Phys. Rev. B **98**, 125416 (2018).
[61]D. B. Litvin, "Magnetic space-group types," Acta Crystallogr., Sect. A **57**, 729–730 (2001).
[62]S. Hayami, Y. Yanagi, and H. Kusunose, "Momentum-dependent spin splitting by collinear antiferromagnetic ordering," J. Phys. Soc. Jpn. **88**, 123702 (2019).
[63]C. C. Ye, K. Tenzin, J. Sławińska, and C. Autieri, "Dominant orbital magnetization in the prototypical altermagnet MnTe," arXiv:2505.08675 (2025).

18 December 2025 09:06:25

© Author(s) 2025